J Nanopart Res (2009) 11:25–39
DOI 10.1007/s11051-008-9419-7

Toxicity of nano- and micro-sized ZnO particles in human lung epithelial cells

Weisheng Lin · Yi Xu · Chuan-Chin Huang · Yinfa Ma · Katie B. Shannon · Da-Ren Chen · Yue-Wern Huang

Received: 22 April 2008 / Accepted: 18 May 2008 / Published online: 10 June 2008
© Springer Science+Business Media B.V. 2008

Abstract This is the first comprehensive study to evaluate the cytotoxicity, biochemical mechanisms of toxicity, and oxidative DNA damage caused by exposing human bronchoalveolar carcinoma-derived cells (A549) to 70 and 420 nm ZnO particles. Particles of either size significantly reduced cell viability in a dose- and time-dependent manner within a rather narrow dosage range. Particle mass-based dosimetry and particle-specific surface area-based dosimetry yielded two distinct patterns of cytotoxicity in both 70 and 420 nm ZnO particles. Elevated levels of reactive oxygen species (ROS) resulted in intracellular oxidative stress, lipid peroxidation, cell membrane leakage, and oxidative DNA damage. The protective effect of *N*-acetylcysteine on ZnO-induced cytotoxicity further implicated oxidative stress in the cytotoxicity. Free Zn^{2+} and metal impurities were not major contributors of ROS induction as indicated by limited free Zn^{2+} cytotoxicity, extent of Zn^{2+} dissociation in the cell culture medium, and inductively-coupled plasma-mass spectrometry metal analysis. We conclude that (1) exposure to both sizes of ZnO particles leads to dose- and time-dependent cytotoxicity reflected in oxidative stress, lipid peroxidation, cell membrane damage, and oxidative DNA damage, (2) ZnO particles exhibit a much steeper dose–response pattern unseen in other metal oxides, and (3) neither free Zn^{2+} nor metal impurity in the ZnO particle samples is the cause of cytotoxicity.

Keywords ZnO · Particles · Oxidative stress · Lipid peroxidation · Oxidative DNA damage · Human bronchoalveolar carcinoma-derived cell (A549) · Nanotechnology · Occupational health · EHS

W. Lin · Y. Ma
Department of Chemistry and Environmental Research Center, Missouri University of Science and Technology, 400 W. 11th Street, Rolla, MO 65409, USA

Y. Xu · C.-C. Huang · K. B. Shannon · Y.-W. Huang (✉)
Department of Biological Sciences and Environmental Research Center, Missouri University of Science and Technology, 400 W. 11th Street, Rolla, MO 65409, USA
e-mail: huangy@mst.edu

D.-R. Chen
Department of Energy, Environmental and Chemical Engineering, Washington University in St. Louis, Campus Box 1180, One Brookings Drive, St. Louis, MO 63130, USA

Introduction

The U.S. National Nanotechnology Initiative defines nanomaterials as materials that have at least one dimension in the range of 1–100 nm. Significant increases in production and demand could lead to unintended exposures to nanomaterials by occupational workers and/or end product users via inhalation, dermal absorption, and gastrointestinal

tract absorption. Because of their unique properties, including small size and corresponding large-specific surface area (SSA), nanomaterials are hypothesized to impose different degrees of biological effects from their micro-scaled materials (Oberdorster et al. 2005; Kipen and Laskin 2005; Nel et al. 2006). The extent of exposure and resulting adverse effects on human health and the environment remain largely unknown (Dreher 2004; Jeng and Swanson 2006).

Nanostructures of ZnO, including particles, rods, wires, belts, tubes, cages, walls, and rings, have attracted a great deal of attention in recent years because of their useful electronic and optoelectronic properties and novel applications in catalysis, paints, wave filters, UV detectors, transparent conductive films, varistors, gas sensing, solar cells, sunscreens, and other cosmetic products (Ramakrishna and Ghosh 2003; Bae and Seo 2004; Comini et al. 2002; Bai et al. 2003; Ding and Wang 2004; Zhu et al. 2005; Huang et al. 2006). The toxicity of ZnO particles has been studied in rats (Hirano et al. 1989), mice (Wesselkamper et al. 2001, 2005), guinea pigs (Lam et al. 1985), and ferrets (Straube et al. 1980). Several studies showed that inhalation of low levels of ZnO nanoparticles (median diameter 50 nm) in guinea pigs causes significant pulmonary function changes and damage (Lam et al. 1988; Conner et al. 1988). Metallothionein and heme oxygenase in rat lungs are induced following inhalation exposure to 2.5 and 5.0 mg/m^3 ZnO fume (median diameter 60 nm) (Cosma et al. 1992). Inhalation of ZnO causes pulmonary impairment and systemic effects such as metal fume fever in humans (Fine et al. 1997). The recommended threshold limit values of ZnO for welders and others in the workplace have been set at 5 mg/m^3 (Beckett et al. 2005).

In this study, we hypothesize that (1) 70 nm ZnO particles are more cytotoxic than 420 nm ZnO particles due to their smaller size and greater SSA and (2) ZnO particles' cytotoxicity is a result of oxidative stresses that can be prevented by treatment with antioxidant *N*-acetylcysteine (NAC). We also evaluated the possible contribution of free zinc ion (Zn^{2+}) released from ZnO and metal impurities in ZnO nanoparticles to the cytotoxicity and propose two alternative possible chemical mechanisms of toxicity. Finally, we demonstrate that ZnO cytotoxicity differs from that caused by various other metal oxides.

Materials and methods

ZnO particles

Both 70 and 420 nm ZnO particles were purchased from Sigma (Saint Louis, MO, USA) at >99.0% purity. The following characterization was performed in a dry state. Particle size distributions were measured by Philips EM430 transmission electron microscopy (TEM) (Philips Electron Optics, Eindhoven, Holland). Crystal structure was characterized using a Scintag XDS 2000 diffractometer (Scintag, Inc., Cupertino, CA, USA). Particle SSA was determined using a Quantachrome Autosorb 1-C (Boynton, FL, USA). The characterization data were shown in Table 1.

Trace metal impurities in 70 and 420 nm ZnO particles were measured using a Perkin–Elmer ELAN DRC-e inductively-coupled plasma-mass spectrometry (ICP-MS) system (Perkin–Elmer, Wellesley, MA, USA). The ICP-MS conditions were set up as follows: vacuum pressure: 6.5×10^{-6} torr; nebulizer gas flow: 0.98 L/min; ICP RF power: 1,200 W; lens voltage: 7.6 V; analog stage voltage: −1,700 V; pulse stage voltage: 1,100 V. The data were presented in Table 2.

Suspensions of ZnO particles were prepared in the cell culture medium with serum and dispersed using a Fisher sonicator FS-60H (Fisher Scientific, Pittsburg, PA, USA) for 5 min. In each study, the suspension was freshly prepared, diluted to desired concentrations in serum-containing medium, and then immediately applied to the human bronchoalveolar carcinoma-derived cells (A549). Due to their nanoscale size and surface property, ZnO nanoparticles tend to aggregate or precipitate in suspensions. Thus, we measured hydrodynamic sizes of ZnO particles in cell medium at 100 μg/mL (stock solution) and a series of diluted concentrations to 10 μg/mL by dynamic light scattering (DLS) using a Nanotrac NPA250 (Microtrac, North Largo, FL, USA).

Chemicals

Fetal bovine serum was purchased from American Type Culture Collection (ATCC) (Manassas, VA, USA). Ham's F-12 medium with L-glutamine, HPLC grade *n*-butanol, acetonitrile, and analytical grade 12 M hydrochloric acid were purchased from Fisher Scientific

Table 1 Characterization of ZnO particles of 70 and 420 nm. Size, SSA, and crystalline structure were determined by TEM, BET surface area analyzer, and XRD, respectively

ZnO (nm)	Size and distribution nm (mean ± SD)	SSA (m^2/g)	Crystalline structure
70	70 ± 13 ($N = 50$)	12.16	Hexagonal
420	420 ± 269 ($N = 70$)	8.61	Hexagonal

Table 2 Metal impurity levels in ZnO particles of 70 and 420 nm tested in an ICP-MS system. The detection limit is 0.04 ppm[a]

Elements	Metal impurity levels (ppm)	
	70 nm ZnO	420 nm ZnO
Na	45.4	7.5
K	44.9	4.4
Cu	37.9	9.3
Se	18.2	18.7
Ca	8.6	1.7
As	5.5	5.7
Pb	2.9	4.6
Mg	2.4	0.5
Cd	1.4	2.8
Ga	0.8	0.7
Al	0.6	0.3
Sb	0.3	0.2
Ti	0.2	ND[b]
Ni	0.1	ND[b]
Ag	0.1	0.1
Ba	0.1	ND[b]
Rb	0.07	ND[b]
Cr	0.04	0.05
Total	169.5	56.6
Be, Fe, V, Mn, Co, Sr, Mo, Cs, Ti, U	ND[b]	

[a] One part per million (ppm) of a specific metal is defined as 1 g of that metal per 10^6 g of ZnO

[b] Not detected

(Pittsburgh, PA, USA). Trypsin-EDTA (1×) and Hank's balanced salt solution (HBSS) were purchased from Invitrogen Co. (Carlsbad, CA, USA). Sulforhodamine B was purchased from ICN Biomedicals (Irvine, CA, USA). Penicillin–streptomycin, trichloroacetic acid (TCA), 1,1,3,3-tetramethoxypropane, 2-thiobarbituric acid, *o*-phosphoric acid (HPLC grade), *N*-(1-pyrenyl) maleimide, 2′, 7′-dichlorofluorescin diacetate (DCFH-DA), NAC, glutathione (reduced), L-serine, boric acid, diethylenetriaminepentaacetic acid (DETAPAC), TRIS hydrochloride, butylatedhydroxytoluene (BHT), tetrahydrofuran, Na_2HPO_4, NaH_2PO_4, and acetic acid (HPLC grade) were obtained from Sigma–Aldrich (Saint Louis, MO, USA). Ultrapure DI-water was prepared using a Milli-Q system (Millipore, Bedford, MA, USA).

Cell culture and treatment with ZnO particles

The human bronchoalveolar carcinoma-derived cell line (A549) was purchased from ATCC (Manassas, VA, USA). This cell line has been widely used in in vitro particulate matter-related pulmonary toxicity studies (Wottrich et al. 2004; Upadhyay et al. 2003; Huang et al. 2004). Cells were maintained in Ham's F-12 medium supplemented with 5% fetal bovine serum, 100 units/mL penicillin, and 100 μg/mL streptomycin, and grown at 37 °C in a 5% CO_2 humidified environment. A549 cells were seeded into 24 well plates and allowed to attach for 48 h. Cell densities followed the recommendation from the ATCC protocol as well as sensitivity and detection limits of analytical instrument. Freshly dispersed particles suspensions in cell culture medium were diluted to desired concentrations and immediately applied to the cells. Approximately 20,000 cells/cm^2 were present when nanoparticle suspensions were dispensed. Cells without ZnO particles were used as the control in each experiment. SiO_2, which has been shown to be toxic to A549 cells in our previous study (Lin et al. 2006a, b), was included as a positive control.

A stock solution up to 100 μg ZnO/mL cell medium was prepared to yield a more accurate weighing of ZnO powder. A range of concentrations between 8 and 25 μg/mL was initially tested. A steep, dose-dependent toxicity was noted between 8 and 18 μg/mL. Time-dependent responses were measured at 6, 12, and 24 h. Three concentrations of ZnO, representing low, medium, and high cytotoxicity, were then used in the subsequent experiments to measure biomarkers of oxidative stress and DNA damage.

In order to further establish the role of oxidative stress in the cytotoxicity, cells were co-treated 14 μg/mL ZnO with or without NAC at nontoxic levels for 24 h followed by a cell viability assay. After incubation with ZnO particles for 24 h, cells or cell culture medium was collected for analysis. A serine borate buffer was used

during cell homogenation to prevent spurious oxidation in the GSH and lipid peroxidation assays. The buffer contained 100 mM Tris–HCl, 10 mM borate, 5 mM serine, and 1 mM DETAPAC with the final pH adjusted to 7.0 using concentrated NaOH. The cell samples are homogenized in the buffer with a tissue homogenizer (Model 985-370, type 2, Biospec Products) on ice for 2 min, with 5 s intervals of homogenization. Homogenates were frozen at −70 °C until analyzed.

Cytotoxicity measurement

At the end of cell exposure to ZnO suspensions, the medium was discarded and the SRB assay was used to determine cell viability relative to the control group (Skehan et al. 1990). Briefly, the cells were fixed with cold 10% TCA for 1 h at 4 °C environment. The TCA solution was then discarded, and the cells were washed thrice with distillated water followed by complete drying. Sulforhodamine B (0.2% in a 1% acetic acid) was added to stain the cells for 30 min at room temperature. The staining solution was discarded and the cells were washed with 1% acetic acid to eliminate excess dye. After complete drying, the dye was dissolved in cold 10 mM Tris buffer (pH 10.5). One hundred microliter aliquots of dye solution were transferred into a 96-well plate and the absorbance was measured at 550 nm using a microplate reader (FLOURstar, BMG Labtechnologies, Durham, NC, USA).

Lactate dehydrogenase measurement

Lactate dehydrogenase (LDH) activity in the cell culture medium was determined by an LDH Kit (Pointe Scientific, Lincoln Park, MI, USA). One hundred microliter of culture supernatant was used for analysis. LDH catalyzed the oxidation of lactate to pyruvate with simultaneous reduction of NAD^+ to NADH. The rate of NAD^+ reduction was directly proportional to LDH activity in the cell medium. Absorption was measured using a Beckman DU-640B UV–Visible Spectrophotometer at 340 nm.

Intracellular reactive oxygen species measurement

Intracellular reactive oxygen species (ROS) generation was measured using a well-characterized probe, 2′-, 7′-DCFH-DA (Wang and Joseph 1999). DCFH-DA is hydrolyzed by esterases to DCFH, which is trapped within the cell. This nonfluorescent molecule is then oxidized to fluorescent DCF by action of cellular oxidants. A DCFH-DA stock solution (in methanol) of 10 mM was diluted 500-fold in HBSS without serum or other additive to yield a 20 μM working solution. Cells were washed twice with HBSS and then incubated with DCFH-DA working solution for 1 h at dark environment (37 °C incubator) followed by treatment with ZnO particles for 24 h. After exposure, fluorescence was determined at 485 nm excitation and 520 nm emission using a microplate reader (FLOURstar, BMG Labtechnologies, Durham, NC, USA).

Measurement of GSH (reduced glutathione)

HPLC was used to determine the cellular GSH levels (Winters et al. 1995). Cells were homogenized in serine borate buffer (100 mM Tris–HCl, 10 mM boric acid, 5 mM L-serine, 1 mM DETAPAC, pH 7.5). Twenty microliter homogenate was added to 230 μL HPLC grade H_2O and 750 μL NMP solution (1 mM in acetonitrile). The resulting suspensions were incubated for 5 min at room temperature, and then 5 μL of 2 N HCl was added to stop the reaction. The samples were filtered through a 0.2 μm Whatman Puradisc syringe filter (Whatman International, Maidstone, Kent, UK), and an aliquot of 20 μL was injected for analysis using a Perkin–Elmer HPLC system (Perkin–Elmer, Wellesley, MA, USA) with fluorescence detection (excitation at 330 nm, emission at 375 nm) and a 5-μm Reliasil C18 column (250 × 4.6 mm^2; Column Engineering, Ontario, CA, USA). The mobile phase consisted of 70% acetonitrile and 30% HPLC H_2O containing 1 mL/L acetic acid and 1 mL/L *o*-phosphoric acid. The flow rate was 1.0 mL/min.

Lipid peroxidation measurement

The extent of cellular lipid peroxidation was determined by measuring the concentrations of thiobarbituric acid-reactive substances (TBARS). An aliquot of 350 μL of cell homogenate was mixed with 100 μL of 500 ppm BHT in methanol and 550 μL of 10% TCA. The resulting mixture was boiled for 30 min to precipitate the proteins. After cooling on ice, the sample was centrifuged at 1,500*g*

for 10 min. The supernatant was collected, and 500 μL was mixed with 500 μL of a saturated aqueous TBA solution. This mixture was heated in a boiling water bath for 30 min. After cooling to room temperature, 500 μL samples were extracted with 1 mL of *n*-butanol using a Vortex mixer, and then centrifuged at 1,000*g* for 5 min. The top layer was collected and filtered through a 0.2 μm Whatman Puradisc syringe filter, followed by analysis with the same Perkin–Elmer HPLC system and column that was used for GSH analysis. Excitation wavelength and emission wavelength were set at 515 and 550 nm, respectively. Twenty microliter samples were injected for analysis. The mobile phase consisted of 69.4% 5 mM sodium phosphate buffer (pH 7.0), 30% acetonitrile, and 0.6% THF. The flow rate of mobile phase was 1.0 mL/min.

Oxidative DNA damage measurement (single-cell gel electrophoresis)

The single-cell gel electrophoresis (comet assay) was performed using the Trevigen's comet assay kit (Trevigen, Gaithersberg, MD, USA). After treatment with ZnO particles for 24 h, the cells were rinsed with ice-cold 1× PBS and trypsinized. Then the cells were washed once in ice-cold 1× PBS and resuspended at 1×10^5 cells/mL in ice-cold 1× PBS. An aliquot of 10 μL cell suspension was mixed with 100 μL molten agarose (37 °C), and 75 μL of this mixture was immediately applied to a glass slide. The slide was held horizontal at 4 °C for 30 min to improve adherence. Then the slide was immersed in cold lysis solution to lyse the cells. After 50 min at 4 °C in the dark, the slide was immersed in an alkaline solution (300 mM NaOH, 1 mM EDTA, pH > 13) at room temperature in the dark to denature the DNA. After 30 min, the slide was placed on a horizontal electrophoresis unit and the unit was filled with fresh buffer (300 mM NaOH, 1 mM EDTA, pH > 13) to cover the slide. Electrophoresis was conducted at 27 V (300 mA) for 40 min at 4 °C in the dark. The slide was then washed gently with distilled water and immersed in 70% ethanol for 5 min. After the slide was air dried, 50 μL of SYBR green I working solution was applied to each circle of dried agarose. All steps described above were conducted under yellow light to prevent additional DNA damage.

Slides were viewed using an epifluorescence Olympus IX 51 microscope (Olympus America, Center Valley, PA, USA) equipped with a fluorescein filter. Observations were made at a final magnification of 400×. Thirty randomly selected cells per experimental point were imaged and analyzed using SlideBook 4.1 software (Intelligent Imaging Innovations, Denver, CO, USA). Results were reported as tail DNA percentage, a parameter describing the number of migrated fragments, represented by the fluorescence intensity in the tail, expressed as the mean of the 30 cells.

Subcellular localization of ZnO particles

A549 cells were plated into 100 cm^2 Petri dishes at a density of 8.0×10^5 cells per dish in 13 mL culture medium and allowed to attach for 48 h. The cells were treated with 70 nm ZnO (12 μg/mL) for 24 h. Following exposure, treated cells were washed with 0.1 M phosphate buffer, fixed with 2% glutaraldehyde and 2% paraformaldehyde in 0.1 M cacodylate buffer, pH 7.2, at 4 °C for 1 h, post-fixed in 1% OsO_4 in 0.1 M phosphate buffer for 1 h, dehydrated in ascending grades of ethanol, and subsequently embedded in epoxy resin. Ultrathin sections (80 nm) were cut en face with a diamond knife, stained with uranyl acetate and lead citrate, and examined using a JEOL 1400 Transmission Electron Microscope.

Protein assay

The total protein concentration was measured by the Bradford method (Bradford 1976) using a BioRad Assay Kit (BioRad, Richmond, CA, USA) and bovine serum albumin as the standard.

Cytotoxicity of Zn^{2+}

In order to test whether cytotoxicity of ZnO nanoparticles is due to Zn^{2+} ions released from ZnO NPs, cells were treated without or with $ZnSO_4$ at 2, 4, 8, 10, and 16 μg/mL. Cytotoxicity was evaluated using the SRB method.

Statistical analysis

IC50 values of each dose–response curve was calculated from the equation, $Y = \text{BOTTOM} + (\text{Top} - \text{Bottom})/$

$(1 + 10^{x-\text{LogEC50}})$. This equation takes into account both highest and lowest responses. One-tailed or two-tailed unpaired Student's *t*-test was used for significance testing with $p = 0.05$. IC50 values of ZnO were acquired by using the software GraphPad Prism 4.0 (GraphPad Software, San Diego, CA, USA). Data were expressed as the mean ± SD from three independent experiments.

Results

Particle characterization and hydrodynamic size in the cell culture medium

The particle mean size and distribution of ZnO measured by TEM were 70 ± 13 ($N = 50$) and 420 ± 269 nm ($N = 70$), respectively. The surface areas of 70 and 420 nm ZnO measured by the BET method were 12.16 and 8.61 m^2/g, respectively. The X-ray diffraction (XRD) analysis clearly showed the hexagonal structure of these two particles (Table 1 and Fig. 1). In order to measure the extent of particle aggregation in cell culture medium, we determined particle's hydrodynamic size using a DLS method (Fig. 2). Two different measurement settings yielded somewhat differing results. In general, the size distributions were not much different between 10 and 50 μg/mL. However, a difference was observed at the highest concentration 100 μg/mL (see more in "Discussion" section). The typical 28 metal impurity levels in ZnO particles tested by an ICP-MS system are shown in Table 2. The overall purity of both particles is greater than 99.98%. The 70 nm ZnO nanoparticles contained a higher total level of metal impurity (169.5 ppm) than the 420 nm ZnO particles (56.6 ppm). It is noteworthy that the levels of iron, a possible ROS inducer via Fenton reaction, were below detection limit (40 ppb) in both sizes of particle samples.

Dose- and time-dependent cytotoxicity of ZnO particles

A series of images from TEM showed that 70 nm ZnO nanoparticle agglomerates were located in vesicles (Fig. 3; images from 420 nm particles not shown). Occasionally, agglomerates were more diffusely, suggesting a possible release of agglomerates from the vesicles. Agglomerates were not found within nucleus or mitochondria.

Exposure of A549 cells to ZnO particles (70 and 420 nm) was characterized by a steep response pattern. Cell viability was reduced by 75–85% between 18 and 25 μg/mL with either size of ZnO (Fig. 4). Studies performed by two independent experimenters showed similar patterns of response; as well, a third experimenter conducting a portion of the same experiments confirmed the similar patterns (data not shown). ZnO initiated cytotoxicity around 8–10 μg/mL with a steep decline in cell numbers between 10 and 18 μg/mL (Fig. 5). ZnO of 70 nm at dosage levels of 8, 10, 12, 14, 16, and 18 μg/mL decreased cell viability to ~94, 84, 65, 48, 30, and 18%, respectively, in comparison to the control group (p's < 0.05). The dose–response curve of the 420 nm ZnO particles showed a similar trend; 8, 10, 12, 14, 16, and 18 μg/mL levels reduced cell viability to 88, 83, 68, 52, 36, and 28%, respectively (p's < 0.05).

Cytotoxicity of ZnO particles of either size did not differ from each other in the concentration range of 10–16 μg/mL. The EC50 values of 70 and 420 nm ZnO particles are 13.6 and 14.2 μg/mL, respectively (Fig. 6a). Mass-based dosages were converted to particle SSA (m^2/mL) (SSA)-based dosages, and the cell viability was replotted in Fig. 6b. With the same SSA, 420 nm ZnO is more toxic than 70 nm ZnO (p's < 0.05).

Time course experiments revealed that toxicity induced by either size of ZnO occurred between 6 and 12 h (Fig. 7). A more pronounced toxicity was observed at 24 h.

Oxidative stress, lipid peroxidation, and cell membrane leakage induced by ZnO particles

In order to examine oxidative stress and lipid peroxidation, we selected 10, 12, and 14 μg/mL concentrations representing low, medium, and high dosage levels, respectively. DCF fluorescence intensity, indicative of the intracellular level of ROS, increased after 24 h exposure to both ZnO particles (70 and 420 nm) at all concentrations examined. In comparison with the control group, DCF fluorescence intensity of the 70 nm groups increased by 24.4, 28.0, and 57.2%, respectively (p's < 0.05). The DCF fluorescence intensity of the 420 nm ZnO group, which increased by 17.3, 19.0, and 42.5%, was not

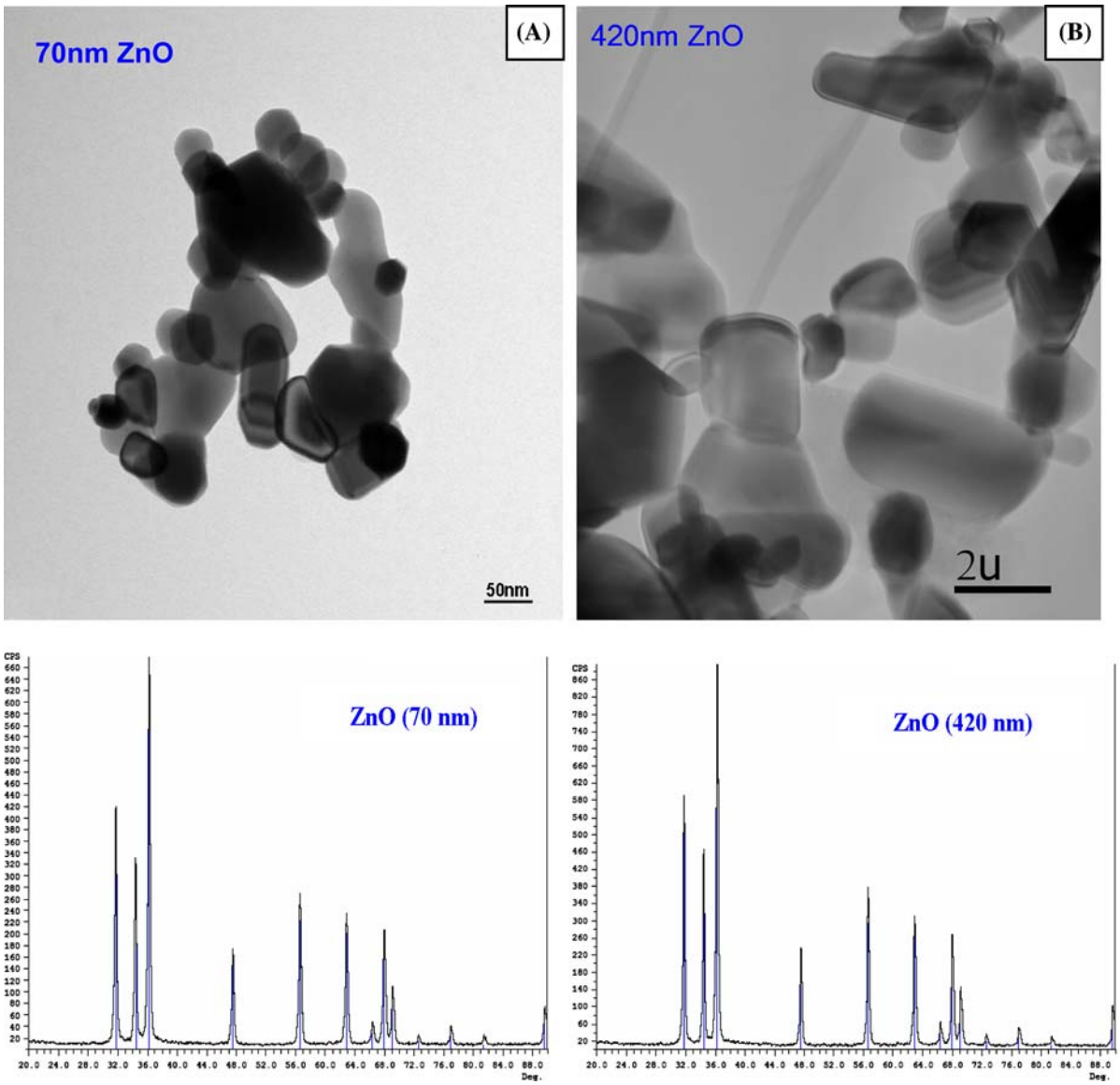

Fig. 1 TEM images and XRD analysis of ZnO particles. (**a**) 70 nm ZnO particles; (**b**) 420 nm ZnO particles. XRD analysis indicated both particles were hexagonal

significantly different from that of their respective 70 nm ZnO group (p's > 0.05) (Fig. 8a). Cellular GSH level exhibited a dose-dependent decrease (Fig. 8b). The GSH levels were reduced by 8.6, 24.6, and 54.4% after 24 h exposure to 70 nm ZnO at all exposure levels examined. Similarly, the GSH levels were reduced by 5.7, 17.8, and 42.8%, after exposure to 420 nm ZnO. A 70 nm ZnO at 14 μg/mL dosage level resulted in a significantly lower level of GSH than that of 420 nm ZnO particles ($p < 0.05$), while there were no significant differences at the other two (lower) dosage levels with the different sized particles (p's > 0.05).

In comparison with the control group, the cellular levels of TBARS, a lipid peroxidation indicator, were increased by 170 and 145% after exposure to 14 μg/mL of 70- and 420 nm ZnO for 24 h (p's < 0.05), respectively (Fig. 8c); 70 nm ZnO induced a higher TBARS level than that of 420 nm ZnO particle ($p < 0.05$). The TBARS levels at the two lower concentrations, 10 and

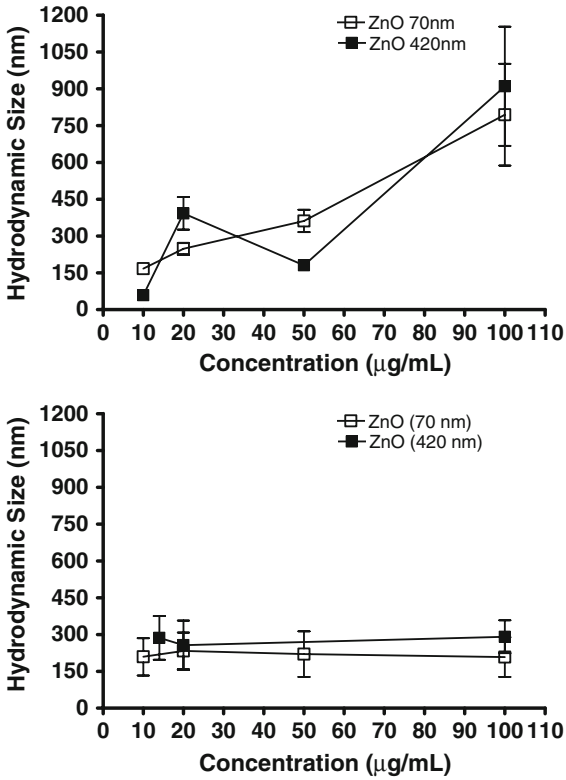

Fig. 2 Hydrodynamic sizes of ZnO particles from two different measurement settings. Each data point in the upper panel was from the average of four consecutive measurements in 5 min. The lower panel was from the average of three independent measurements in three consecutive minutes

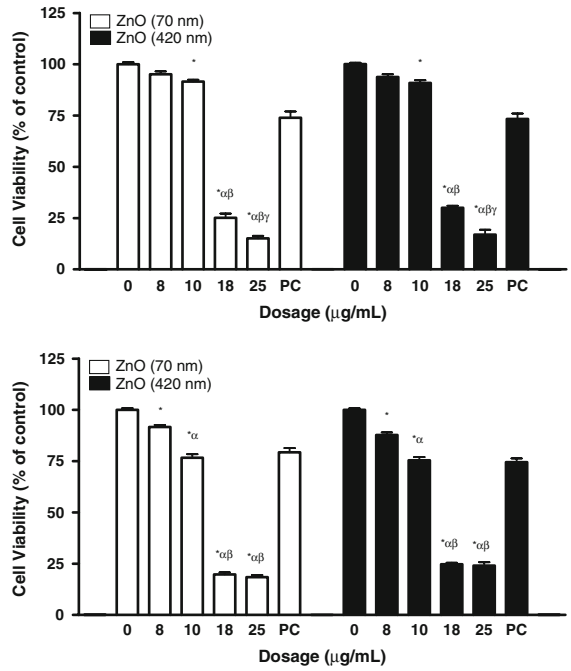

Fig. 4 Exposure of A549 cells to various concentrations of ZnO particles resulted in a steep cell viability reduction pattern. The upper and lower panels conducted by two independent students showed similar patterns. PC, positive control (SiO_2). Values are mean ± SD from three independent experiments. Triplicates of each treatment group were used in each independent experiment. Significance indicated by: * $p < 0.05$ vs. control cells; $^{\alpha}$ $p < 0.05$ vs. cells exposed to 8 μg/mL; $^{\beta}$ $p < 0.05$ vs. cells exposed to 10 μg/mL

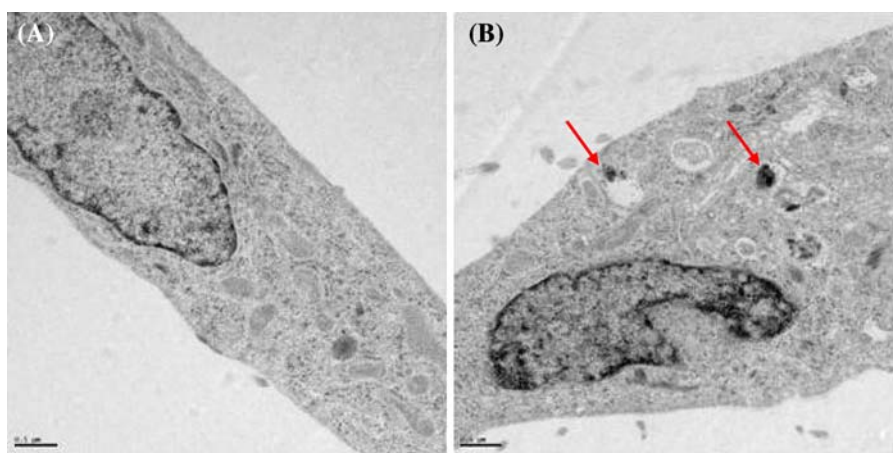

Fig. 3 TEM images of ZnO subcellular localization. (**a**) control; (**b**) cells treated with 12 μg/mL of 70 nm ZnO. Arrows pointed to nanoparticle agglomerates in vesicles. The size of the bar of both images is 0.5 μm

12 μg/mL, were not significantly different from the control group level (p's > 0.05). Cell membrane leakage was reflected in the elevated LDH levels in cell culture medium after cells were exposed to both particle sizes of ZnO for 24 h (Fig. 8d). The LDH levels were increased by 43.1 and 85.3% following exposure to 70 nm ZnO nanoparticles at 12 and 14 μg/mL, respectively (p's < 0.05). In comparison, only at 14 μg/mL

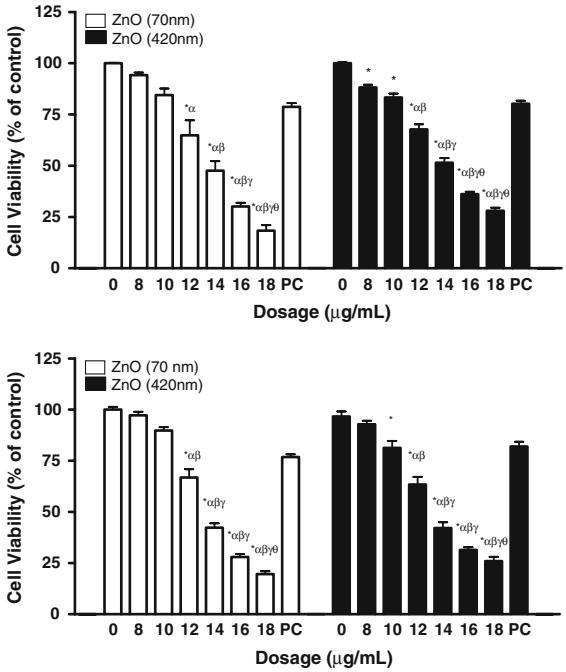

Fig. 5 Exposure of A549 cells to 70 and 420 nm ZnO particles resulted in a dose-dependent cytotoxicity in a narrow range between 8 and 18 μg/mL. The upper and lower panels conducted by two independent students showed similar patterns. PC, positive control (SiO_2). Values are mean ± SD from three independent experiments. Triplicates of each treatment group were used in each independent experiment. Significance indicated by: * $p < 0.05$ vs. control cells; $^{\alpha}$ $p < 0.05$ vs. cells exposed to 8 μg/mL; $^{\beta}$ $p < 0.05$ vs. cells exposed to 10 μg/mL; $^{\gamma}$ $p < 0.05$ vs. cells exposed to 12 μg/mL; $^{\theta}$ $p < 0.05$ vs. cells exposed to 14 μg/mL; $^{\rho}$ $p < 0.05$ vs. cells exposed to 16 μg/mL

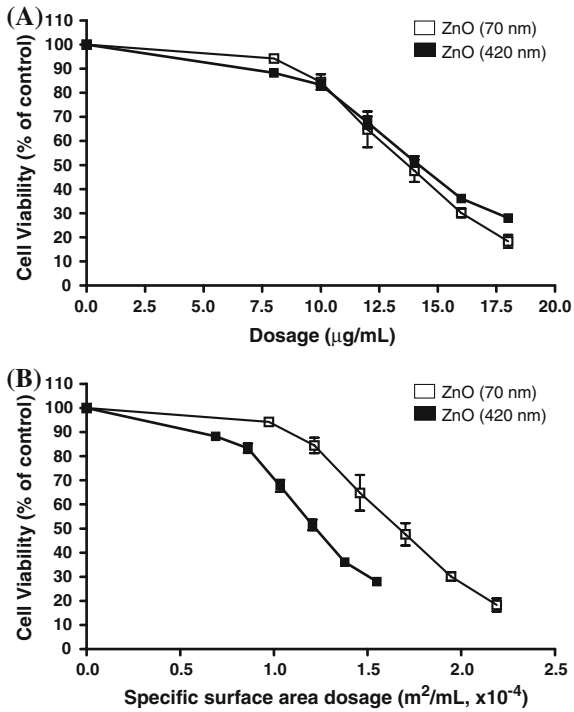

Fig. 6 A549 viability, based on the SRB assay, after 24 h exposure to 10, 12, 14, or 16 μg/mL of ZnO of 70 nm or 420 nm using (**a**) particle mass or (**b**) particle SSA as dosimetry. Cell density data were provided in the text for unit conversion purpose

did 420 nm ZnO cause a significant (52%) elevation of LDH. Exposure to 70 nm ZnO particles induced a higher LDH increase than 420 nm ZnO particles at both 12 and 14 μg/mL dosage levels (p's < 0.05).

NAC reduces cytotoxicity induced by ZnO particles

In order to further establish oxidative stress as the mechanism of ZnO cytotoxicity, a known antioxidant, NAC, was used to co-treat the cells. A dose-dependent cytotoxicity experiment indicated that NAC was not toxic to cells at doses below 1.0 mM (data not shown). In the presence of 0.1, 0.3, and 0.5 mM of NAC, the viability of 70 nm ZnO-treated cells significantly increased to 46, 54, 83, and 90%, respectively (Fig. 9). The viability of 420 nm ZnO-treated cells increased to 57, 64, 78, and 86%, respectively, in the presence of 0.1, 0.3, and 0.5 mM of NAC.

Oxidative DNA damage caused by ZnO particles

DNA damage was measured by the comet assay, with formation of a comet tail after electrophoresis indicating DNA damage. Typical fluorescence images after exposure to 70 nm ZnO nanoparticles at 0 (control), 10, 12, and 14 μg/mL dosages for 24 h are shown in Fig. 10a. The intensity of fluorescence in the comet tail increased with nanoparticle dosage. The percentages of tail intensity significantly increased to 38.4, 36.3, and 91.8% after exposure to 10, 12, and 14 μg/mL dosages, respectively, of 70 nm ZnO nanoparticles (Fig. 10b). For 420 nm ZnO particles, the corresponding data were 30.0, 39.5, and 91.4%. Based on statistical analysis, there was no significant difference in DNA damage between the two

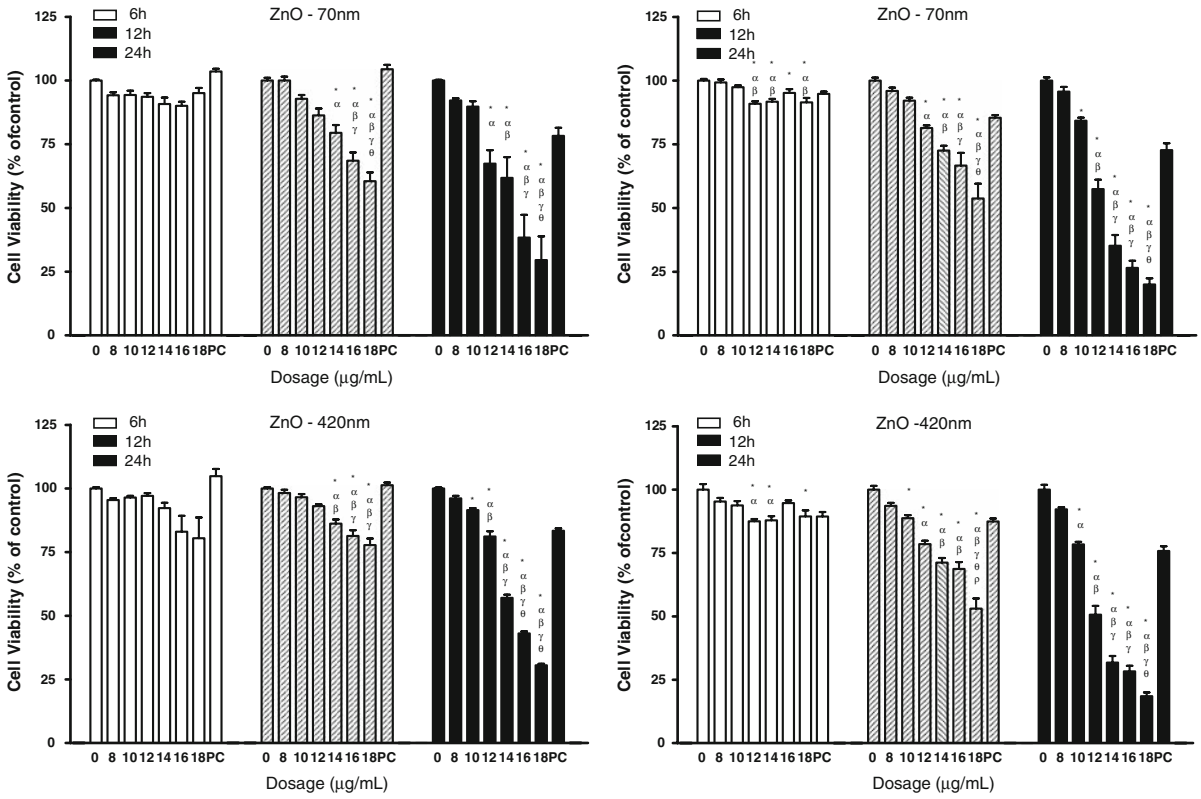

Fig. 7 Time-dependent cytotoxicity of 420 nm ZnO particles. The left two figures and the right two figures were conducted by two independent students. Values are mean ± SD from three independent experiments. Triplicates of each treatment group were used in each independent experiment. The 24-h data in this figure and in Fig. 5 were from independent experiments; both showed high degree of similarity. PC, positive control (SiO_2). * $p < 0.05$ vs. control cells; $^{\alpha}$ $p < 0.05$ vs. cells exposed to 8 μg/mL; $^{\beta}$ $p < 0.05$ vs. cells exposed to 10 μg/mL; $^{\gamma}$ $p < 0.05$ vs. cells exposed to 12 μg/mL; $^{\theta}$ $p < 0.05$ vs. cells exposed to 14 μg/mL; $^{\rho}$ $p < 0.05$ vs. cells exposed to 16 μg/mL

particle sizes in the 10–14 μg/mL dose range. It is worth mentioning that the comet assay can only assess the total DNA damage in a cell and does not distinguish between mtDNA and genomic DNA damage. Due to the small sizes of damaged mtDNAs (2–16 kbp) and small number of copies (100–10,000 copies), it is expected to make a relatively minor contribution to the comet assay.

Cytotoxicity of Zn^{2+}

After A549 cells were exposed to free Zn^{2+} at 2, 4, 8, 10, and 16 μg/mL for 24 h, cell viability decreased to 82.2 and 21.9% at 10 and 16 μg/mL dosages, respectively. Free Zn^{2+} at 2–8 μg/mL did not cause significant cytotoxicity compared to the control (Fig. 11).

Discussion

We compared toxicity of nano- and micro-sized ZnO particles in cultured human bronchoalveolar carcinoma-derived cells. The results indicate that both 70 and 420 nm ZnO particles induce dose-dependent cytotoxicity over a markedly narrow concentration range of 8–18 μg/mL. Cell viability was not particle size dependent at all particle mass-based dosages. Cytotoxicity is time dependent, with a more pronounced response observed at 24 h. The onset of biochemical responses to nanoparticles in early hours of contact remains to be determined.

Strikingly, ZnO possesses a very narrow steep dose–response range (8–18 μg/mL) that is quite different from Al_2O_3 (unpublished data), TiO_2 (unpublished data), and CeO_2 (Lin et al. 2006a, b).

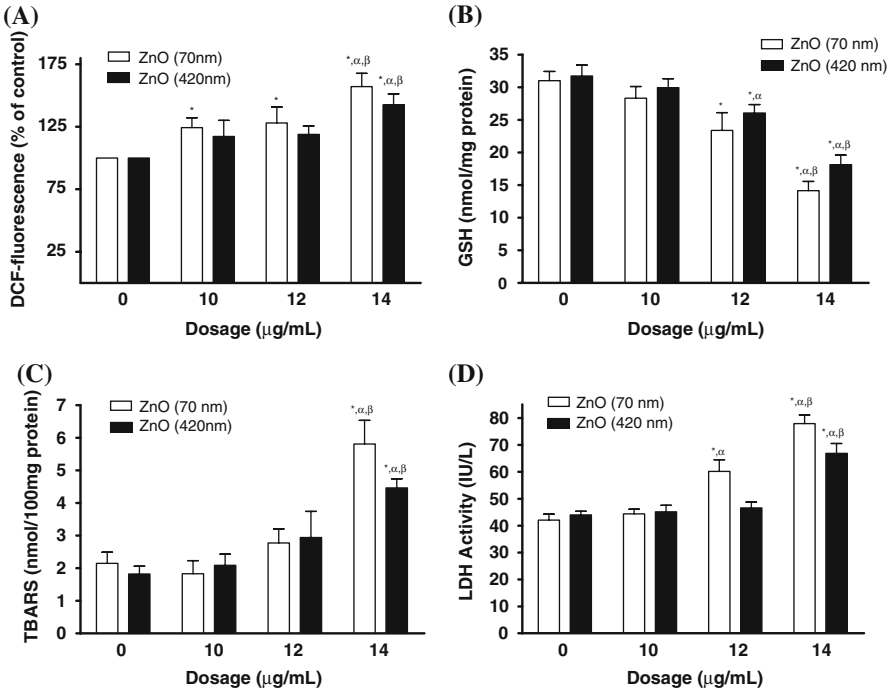

Fig. 8 Biomarkers of oxidative stress and cell membrane leakage in the cells treateds in to 10 with ZnO particles for 24 h. (**a**) DCF-fluorescence intensity, an indication of ROS generation. ROS levels were elevated at all dosages. (**b**) Dose-dependent reduction of cellular GSH levels. (**c**) Lipid peroxidation, as indicated by TBARS. (**d**) LDH activitiethe cell culture medium. Values are mean ± SD from three independent experiments. Triplicates of each treatment group were used in each independent experiment. Significance indicated by: * $p < 0.05$ vs. control cells; $^{\alpha}$ $p < 0.05$ vs. cells exposed 10 μg/mL; $^{\beta}$ $p < 0.05$ vs. cells exposed to 12 μg/mL

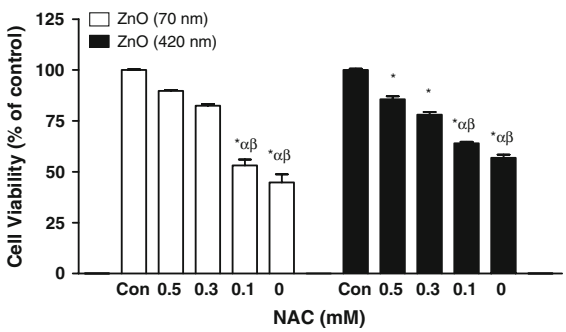

Fig. 9 NAC inhibits cell viability reduction caused by ZnO. Cells were incubated with 14 μg/mL ZnO with or without NAC for 24 h. Values are mean ± SD from three independent experiments. Significance indicated by: * $p < 0.05$ vs. cells exposed to control cells; $^{\alpha}$ $p < 0.05$ vs. cells exposed to 0.5 mM; $^{\beta}$ $p < 0.05$ vs. cells exposed to 0.3 mM

The latter showed more gradual dose–response patterns between 10 and 100 μg/mL, regardless of particle size (Fig. 12). The same steep dose-dependent response of ZnO particles was also observed in BEAS-2B cells (primary and immortalized human epithelial cells), except the cytotoxicity was observed over a slightly lower range of concentrations (6–10 μg/mL; data not shown). Our cell viability data were supported by Jeng and Swanson (2006) that ZnO (50–70 nm) is more toxic than TiO_2, Fe_2O_3, and Al_2O_3 in Neuro-2A cells. The difference in ZnO cytotoxicity between ours and Jeng's is that a steeper response in a narrow range (8–18 μg/mL) was observed in our studies with A549 cells (and BEAS-2B cells), whereas Neuro-2A cells exhibited a dose-dependent response between 10 and 200 μg/mL. At 25 μg/mL of ZnO, the cell number of A549 was reduced by 85%; however, only a 20% reduction of cell number was observed in Neuro-2A cells. The difference observed between Jeng's and ours might be due to the differing cell culture conditions and the cell line sensitivity in cytotoxicity, but not the source of the particles of which were supplied by the same manufacturers. The similarity and difference in findings are informative and critical in establishing

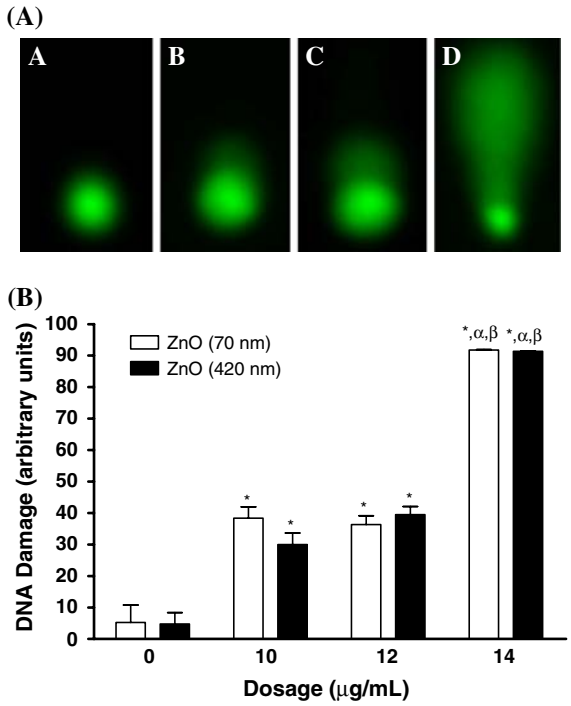

Fig. 10 (**a**) The representative fluorescence images of nuclei treated in the comet assay after 24 h exposure to (**a**) 0 μg/mL, (**b**) 10 μg/mL, (**c**) 12 μg/mL, or (**d**) 14 μg/mL of 70 nm ZnO nanoparticles. (**b**) DNA damage was observed at all dosages. At the same dosage, there was no significant difference in DNA damage between 70 and 420 nm ZnO particles. Values are mean ± SD from three independent experiments. Significance indicated by: * $p < 0.05$ vs. control cells; $^{\alpha}$ $p < 0.05$ vs. cells exposed to 10 μg/mL; $^{\beta}$ $p < 0.05$ vs. cells exposed to 12 μg/mL

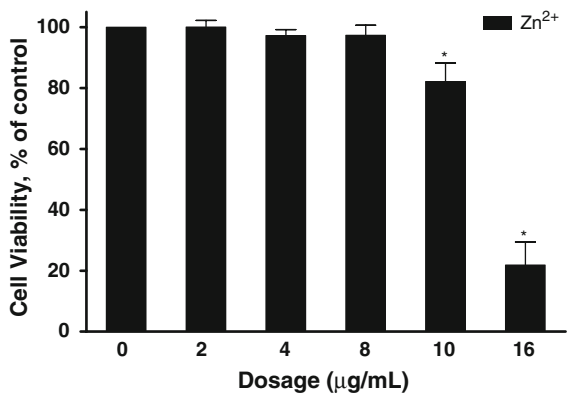

Fig. 11 Viability of A549 cells, based on the SRB assay, after 24 h exposure to 2, 4, 8, 10, or 16 μg/mL of Zn^{2+} ($ZnSO_4$). Values are mean ± SD from three independent experiments. Significance indicated by: * $p < 0.05$ vs. control cells

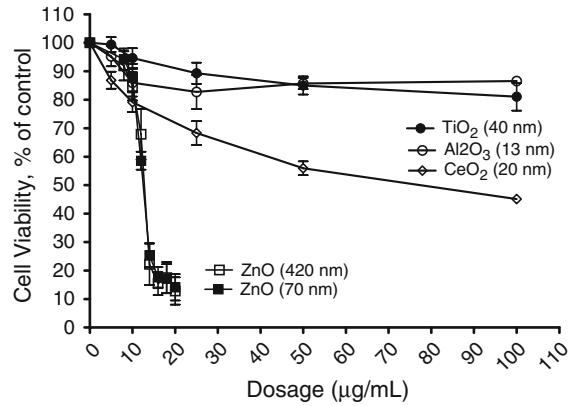

Fig. 12 Cytotoxicity patterns of various metal oxides. ZnO particles have relatively steeper effects on cell viability than other metal oxides. Al_2O_3 and TiO_2 data have not been unpublished, while CeO_2 data were published (Lin et al. 2006a, b)

a different assessment model and management strategy to evaluate risk associated with ZnO exposure.

In general, both sizes of ZnO particles cause similar extents of cellular membrane leakage and oxidative stress as manifested by elevated ROS levels, reduced GSH levels, increased LDH levels, and lipid peroxidation, as well as increased oxidative DNA damage. The critical role of oxidative stress in these actions was supported by the protective effect of NAC on ZnO-induced cytotoxicity, for which NAC acts as a precursor of GSH (Zhang et al. 1999; Cotgreave 1997).

Hydrodynamic size offered a measurement of particle agglomeration in the cell medium. Two measurement settings yielded somewhat different patterns of hydrodynamic sizes. The measured size distributions were not much different between 10 and 50 μg/mL in these two measurement settings, but differed at 100 μg/mL. We noted that particles at higher concentrations were not stable and could precipitate quickly even though untrasonic bath was performed. Our observations imply the need of an aerosol monodisperse system with a real-time monitoring tool to characterize progressive changes during exposure regime. We observed discrepancy between the true physical size and the hydrodynamic size which might be related to the physical principles underlying the two instruments (TEM/XRD versus DLS method). Instead of direct size measurement employed by TEM, DLS measures Brownian movement of particles to estimate diffusion coefficient from which the size of

the suspended particle is estimated using the Stokes-Einstein equation. Anish et al. (2005) also reported that hydrodynamic sizes of nanoparticles could be smaller than their physical sizes.

TEM images revealed nanoparticle agglomerates in intracellular vesicles, presumably a result of endocytosis. In some instances, agglomerates were located more diffusely, possibly indicating the release of agglomerates from the vesicle. Agglomerates were not found in the nucleus or mitochondria. It remains to be elucidated the intracellular locations where toxicity occurs.

Whether smaller particles are more toxic than larger particles of the same chemical composition is a subject of vigorous debate. For nanoparticles of the same chemical composition, size, SSA, and surface properties have been hypothesized to play critical roles in toxicity (Brown et al. 2001; Donaldson and Tran 2002; Oberdorster 2000; Warheit et al. 2006). In this study, particle mass-based and particle SSA-based dosimetries result in two distinct patterns of dose-dependent cytotoxicity. It is not clear how agglomeration may have affected particle transport in cell culture medium (diffusion versus gravitational setting), cellular uptake, and ultimate actual cellular dosage levels (including total particle surface area as "reactive site").

Three chemical mechanisms of free radical induction by ZnO nanoparticles were proposed. First, Zn^{2+} released from ZnO may be a major contributor to toxicity. The results from the free Zn^{2+} toxicity experiment (Fig. 11) indicated that cytotoxicity only occurred at Zn^{2+} concentrations >10 μg/mL. Because of the low dissociation of ZnO in the cell culture medium (Ksp = 3.0×10^{-16}) and the levels of free Zn^{2+} in the control medium and the ZnO-dosed medium were below the detection limit, the possibility of cytotoxicity caused by released Zn^{2+} can be ruled out. Second, impurities (e.g., Cu, Cr, Fe, V, Co) in the particles could induce Fenton or Fenton-like reactions that generate ROS. Low levels of Cu and Cr were detected in particles, while Fe, V, and Co were not detected. Therefore, contribution of metal impurity to toxicity, if any, is expected to be negligible.

Third, based on the potential redox property of glycine-Zn^{2+}/Zn^{+} (or other amino acids-Zn^{2+}/Zn^{+}) in a biological system described by Ai et al. (2003), it is also possible that sequential oxidation–reduction reactions may occur at ZnO particle surface to produce reactive species such as hydrogen peroxide (H_2O_2) and hydroxyl radical ($OH^{\bullet}$). The detailed chemical reactions are under investigation.

Studies have demonstrated that production of H_2O_2 was significantly enhanced in a ZnO particle containing solution when the solution was exposed to UV (300–350 nm) or prevailing laboratory lighting fixture (Russell et al. 1994; Dunford et al. 1997; Shi et al. 1999; Yamamoto et al. 2000; Domenech et al. 2001). On the other hand, in the absence of irradiation or photoactivation, both ZnO and TiO_2 (a photocatalyst) could induce oxidative stress in human neutrophils and bronchial epithelial cells (Gurr et al. 2005; Lindahl et al. 1998). In this study, ZnO particles induced ROS in the absence of irradiation. We would expect that photoactivation effects from the lighting in the cell culture room to be negligible because cells, medium, and particle suspension were kept in the dark environment most of the time. Further, the control group has been used for data adjustment.

In summary, we have demonstrated that 70 and 420 nm ZnO particles significantly reduce cell viability and cause oxidative DNA damage in a dose- and time-dependent manner in A549 cells. The steep response pattern was unexpected and is different from the patterns observed with other metal oxides. The particle mass-based and particle SSA-based dosimetries result in two distinct patterns of cytotoxicity induced by 70 and 420 nm ZnO. The elevated ROS levels, biomarkers of oxidative stress, and the protective effect exerted by NAC support the role of oxidative stress in the development of the toxicity. Free Zn^{2+} and metal impurity do not appear to be major contributors of ROS induction. Chemical mechanisms producing intracellular ROS remain to be investigated with respect to the mechanism of ZnO nanoparticle cytotoxicity.

Acknowledgments The authors thank the financial support from the Departments of Biological Sciences and Chemistry, Environmental Research Center, and the M S&T cDNA Resource Center at the Missouri University of Science and Technology. The authors thank Honglan Shi for ICP-MS analysis. Robert S. Aronstam contributed to technical editing of this manuscript.

References

Ai H, Bu Y, Han K (2003) Glycine-Zn^{+}/Zn^{2+} and their hydrates: on the number of water molecules necessary to stabilize the zwitterionic glycine-Zn^{+}/Zn^{2+} over the nonzwitterionic ones. J Chem Phys 118(24):10973–10985

Anish T, Michael EM, Craig JH, Brooke VH (2005) Effect of ideal, organic nanoparticles on the flow properties of linear polymers: non-Einstein-like behavior. Macromolecules 38(19):8000–8011

Bae SY, Seo HW (2004) Vertically aligned sulfur-doped ZnO nanowires synthesized via chemical vapor deposition. J Phys Chem B 108(17):5206–5210

Bai XD, Gao PX, Wang ZL, Wang EG (2003) Dual-mode mechanical resonance of individual ZnO nanobelts. Appl Phys Lett 82(26):4806–4808

Beckett WS, Chalupa DF, Pauly-Brown A, Speers DM, Stewart JC, Frampton MW, Utell MJ, Huang LS, Cox C, Zareba W, Oberdörster G (2005) Comparing inhaled ultrafine versus fine zinc oxide particles in healthy adults: a human inhalation study. Am J Respir Crit Care Med 171(10):1129–1135

Bradford MM (1976) A rapid and sensitive method for the quantitation of microgram quantities of protein utilizing the principle of protein-dye binding. Anal Biochem 72:248–254

Brown DM, Wilson MR, MacNee W, Stone V, Donaldson K (2001) Size-dependent proinflammatory effects of ultrafine polystyrene particles: a role for surface area and oxidative stress in the enhanced activity of ultrafines. Toxicol Appl Pharmacol 175(3):191–199

Comini E, Faglia G, Sberveglieri G, Pan Z, Wang ZL (2002) Stable and highly sensitive gas sensors based on semiconducting oxide nanobelts. Appl Phys Lett 81(10):1869–1871

Conner MW, Flood WH, Rogers AE, Amdur MO (1988) Lung injury in guinea pigs caused by multiple exposures to ultrafine zinc oxide: changes in pulmonary lavage fluid. J Toxicol Environ Health 25(1):57–69

Cosma G, Fulton H, DeFeo T, Gordon T (1992) Rat lung metallothionein and heme oxygenase gene expression following ozone and zinc oxide exposure. Toxicol Appl Pharmacol 117(1):75–80

Cotgreave IA (1997) N-acetylcysteine: pharmacological considerations and experimental and clinical applications. Adv Pharmacol 38:205–227

Ding Y, Wang ZL (2004) Structure analysis of nanowires and nanobelts by transmission electron microscopy. J Phys Chem B 108(33):12280–12291

Domenech X, Ayllon JA, Peral J (2001) H_2O_2 formation from photocatalytic processes at the ZnO/water interface. Environ Sci Pollut Res Int 8(4):285–287

Donaldson K, Tran CL (2002) Inflammation caused by particles and fibers. Inhal Toxicol 14(1):5–27

Dreher KL (2004) Health and environmental impact of nanotechnology: toxicological assessment of manufactured nanoparticles. Toxicol Sci 77(1):3–5

Dunford R, Salinaro A, Cai L, Serpone N, Horikoshi S, Hidaka H, Knowland J (1997) Chemical oxidation and DNA damage catalysed by inorganic sunscreen ingredients. FEBS Lett 418(1–2):87–90

Fine JM, Gordon T, Chen LC, Kinney P, Falcone G, Beckett WS (1997) Metal fume fever: characterization of clinical and plasma IL-6 responses in controlled human exposures to zinc oxide fume at and below the threshold limit value. J Occup Environ Med 39(8):722–726

Gurr JR, Wang AS, Chen CH, Jan KY (2005) Ultrafine titanium dioxide particles in the absence of photoactivation can induce oxidative damage to human bronchial epithelial cells. Toxicology 213(1–2):66–73

Hirano S, Higo S, Tsukamoto N, Kobayashi E, Suzuki KT (1989) Pulmonary clearance and toxicity of zinc oxide instilled into the rat lung. Arch Toxicol 63(4):336–342

Huang M, Khor E, Lim LY (2004) Uptake and cytotoxicity of chitosan molecules and nanoparticles: effects of molecular weight and degree of deacetylation. Pharm Res 21(2):344–353

Huang GG, Wang CT, Tang HT, Huang YS, Yang J (2006) ZnO nanoparticle-modified infrared internal reflection elements for selective detection of volatile organic compounds. Anal Chem 78(7):2397–2404

Jeng HA, Swanson J (2006) Toxicity of metal oxide nanoparticles in mammalian cells. J Environ Sci Health Part A 41:2699–2711

Kipen HM, Laskin DL (2005) Smaller is not always better: nanotechnology yields nanotoxicology. Am J Physiol Lung Cell Mol Physiol 289:L696–L697

Lam HF, Conner MW, Rogers AE, Fitzgerald S, Amdur MO (1985) Functional and morphologic changes in the lungs of guinea pigs exposed to freshly generated ultrafine zinc oxide. Toxicol Appl Pharmacol 78(1):29–38

Lam HF, Chen LC, Ainsworth D, Peoples S, Amdur MO (1988) Pulmonary function of guinea pigs exposed to freshly generated ultrafine zinc oxide with and without spike concentrations. Am Ind Hyg Assoc J 49(7):333–341

Lin W, Huang YW, Zhou XD, Ma Y (2006a) In vitro toxicity of silica nanoparticles in human lung cancer cells. Toxicol Appl Pharmacol 217(3):252–259

Lin W, Huang YW, Zhou XD, Ma Y (2006b) Toxicity of cerium oxide nanoparticles in human lung cancer cells. Int J Toxicol 25(6):451–457

Lindahl M, Leanderson P, Tagesson C (1998) Novel aspect on metal fume fever: zinc stimulates oxygen radical formation in human neutrophils. Hum Exp Toxicol 17(2):105–110

Nel A, Xia T, Madler L, Li N (2006) Toxic potential of materials at the nanolevel. Science 311(5767):622–627

Oberdorster G (2000) Toxicology of ultrafine particles: in vivo studies. Trans R Soc Lond A 358(1175):2719–2740

Oberdorster G, Oberdorster E, Oberdorster J (2005) Nanotoxicology: an emerging discipline evolving from studies of ultrafine particles. Environ Health Perspect 113(7):823–839

Ramakrishna G, Ghosh HN (2003) Effect of particle size on the reactivity of quantum size ZnO nanoparticles and charge-transfer dynamics with adsorbed catechols. Langmuir 19(7):3006–3012

Russell J, Ness J, Chopra M, McMurray J, Smith WE (1994) The assessment of the HO scavenging action of therapeutic agents. J Pharm Biomed Anal 12(7):863–866

Shi X, Dong Z, Huang C, Ma W, Liu K, Ye J, Chen F, Leonard SS, Ding M, Castranova V, Vallyathan V (1999) The role of hydroxyl radical as a messenger in the activation of nuclear transcription factor NF-kappaB. Mol Cell Biochem 194(1–2):63–70

Skehan P, Storeng R, Scudiero D, Monks A, McMahon J, Vistica D, Warren JT, Bokesch H, Kenney S, Boyd MR (1990) New colorimetric cytotoxicity assay for anticancer-drug screening. J Natl Cancer Inst 82(13):1107–1112

Straube EF, Schuster NH, Sinclair AJ (1980) Zinc toxicity in the ferret. J Comp Pathol 90(3):355–361

Upadhyay D, Panduri V, Ghio A, Kamp D (2003) Particulate matter induces alveolar epithelial cell DNA damage and apoptosis: role of free radicals and the mitochondria. Am J Respir Cell Mol Biol 29(2):180–187

Wang H, Joseph JA (1999) Quantifying cellular oxidative stress by dichlorofluorescein assay using microplate reader. Free Radic Biol Med 27(5–6):612–616

Warheit DB, Webb TR, Sayes CM, Colvin VL, Reed KL (2006) Pulmonary instillation studies with nanoscale TiO_2 rods and dots in rats: toxicity is not dependent upon particle size and surface area. Toxicol Sci 91(1):227–236

Wesselkamper SC, Chen LC, Gordon T (2001) Development of pulmonary tolerance in mice exposed to zinc oxide fumes. Toxicol Sci 60(1):144–151

Wesselkamper SC, Chen LC, Gordon T (2005) Quantitative trait analysis of the development of pulmonary tolerance to inhaled zinc oxide in mice. Respir Res 6:73

Winters RA, Zukowski J, Ercal N, Matthews RH, Spitz DR (1995) Analysis of glutathione, glutathione disulfide, cysteine, homocysteine, and other biological thiols by high-performance liquid chromatography following derivatization by n-(1-pyrenyl)maleimide. Anal Biochem 227(1):14–21

Wottrich R, Diabate S, Krug HF (2004) Biological effects of ultrafine model particles in human macrophages and epithelial cells in mono- and co-culture. Int J Hyg Environ Health 207(4):353–361

Yamamoto Y, Imai N, Mashima R, Konaka R, Inoue M, Dunlap WC (2000) Singlet oxygen from irradiated titanium dioxide and zinc oxide. Methods Enzymol 319: 29–37

Zhang Z, Shen HM, Zhang QF, Ong CN (1999) Critical role of GSH in silica-induced oxidative stress, cytotoxicity, and genotoxicity in alveolar macrophages. Am J Physiol 277(4 Pt 1):L743–L748

Zhu BL, Xie CS, Zeng DW, Song WL, Wang AH (2005) Investigation of gas sensitivity of Sb-doped ZnO nanoparticles. Materials Chem Phys 89(1):148–153